


## RESEARCH ARTICLE

# Meso-substituted boron-dipyrromethene compounds: synthesis, tunable solid-state emission, and application in blue-driven LEDs

Hao Liu<sup>1</sup> | Huan Su<sup>1</sup> | Zhiyuan Chen<sup>1</sup> | Senqiang Zhu<sup>1</sup> | Rui Liu<sup>1,2</sup>  | Hongjun Zhu<sup>1</sup>

<sup>1</sup>School of Chemistry and Molecular Engineering, Nanjing Tech University, Nanjing, China

<sup>2</sup>Jiangsu Greenscie Chemical Co., Ltd, Zhenjiang, China

**Correspondence**

Rui Liu and Senqiang Zhu, School of Chemistry and Molecular Engineering, Nanjing Tech University, Nanjing 211816, China.  
Email: rui.liu@njtech.edu.cn;  
zhusenqiang1993@njtech.edu.cn

**Funding information**

Natural Science Foundation of Jiangsu Province, Grant/Award Number: BK20170104; Postgraduate Research & Practice Innovation Programme of Jiangsu Province, Grant/Award Number: KYCX20\_1032; 'Six Talent Peaks Project' of Jiangsu Province, Grant/Award Number: XCL-037; National Natural Science Foundation of China, Grant/Award Number: 21602106

**Abstract**

In this work, we depict the synthesis and characterization of a series of *meso*-substituted boron-dipyrromethene (BODIPY) compounds. Their optical and electrochemical properties were investigated systematically. All these compounds exhibited intense absorption bands in the ultraviolet (UV) and visible regions, which arise from the  $\pi$ - $\pi^*$  transitions based on their BODIPY core segments. By comparing electron-withdrawing substituents and electron-donating substituents, we found that these compounds exhibited some similar photophysical properties but exhibited different fluorescence in the solid state. All compounds were highly emissive in dichloromethane at room temperature ( $\lambda_{em} = 512$ – $523$  nm,  $\Phi_{PL} > 0.9$ ). When these compounds were applied in blue-driven light-emitting diodes (LEDs) as light-emitting materials, the devices showed luminescence efficiency ranging from 1.09 to 34.13 lm/W. Their luminescence and electrochemical properties could be used for understanding the structure–property relationship of BODIPY compounds and developing functional fluorescent materials.

**KEYWORDS**

BODIPY, electrochemical properties, emission, light-emitting diodes, synthesis

## 1 | INTRODUCTION

Boron-dipyrromethene (BODIPY) compounds were first reported by Treibs and Kreuzer in 1968,<sup>[1]</sup> and have attracted great interest in the past decades due to their potential applications in photodynamic therapy, molecular probes, nonlinear optical materials, laser dyes, and solar cells.<sup>[2–7]</sup> There is also a huge variety of functionalized BODIPY dyes for studying biochemistry processes in biological systems (DNA, proteins, lipids, and so on).<sup>[8,9]</sup> They have been widely used due to their excellent optical properties including strong ground-state absorption, high-fluorescence quantum yield, and high optical stability.<sup>[10,11]</sup> In addition, adjusting their photophysical properties through structural modifications also provided good opportunities for various functional applications.

The optoelectronic properties of BODIPY compounds are usually adjustable by introducing various substituents. This has led to comprehensive synthetic efforts and the minor adjustment of their optical performance through both theoretical modeling<sup>[12]</sup> and experimental studies.<sup>[13]</sup> BODIPYs with a *meso*-substitution have generated wide research interest due to their special luminescence characteristics.<sup>[14,15]</sup> Different photophysical properties are related to slight changes with the properties of the substituents. For instance, the outstanding fluorescence properties of BODIPY are exhibited in *meso*-substituted alkyl chain cores (photoluminescence quantum yield,  $\Phi_{PL} > 0.9$ ),<sup>[16–18]</sup> but the *meso*-alkenyl derivatives are nearly non-fluorescent ( $\Phi_{PL} \approx 0$ ).<sup>[19]</sup> Research has shown that their excited state relaxation speed caused this phenomenon. The *meso*-phenyl derivatives are different from alkyl and alkenyl derivatives, although they

demonstrate a high-fluorescence quantum yield. However, the molecular structure is key to controlling their luminescence.

Although the BODIPY compound has excellent photophysical properties, it is still at a disadvantage for the application of light-emitting devices. The main factor that restricts traditional BODIPYs in luminescence displays and illumination is its weak fluorescence, and even aggregation-caused quenching (ACQ) occurs in the solid state or an aggregation state. The cause of ACQ is that BODIPYs with a flat and rigid construction behave unfavourably in intermolecular interactions (e.g.  $\pi$ - $\pi$  stacking) in the solid state, which seriously affects the application of this series of compounds in organic light-emitting materials. To reduce the ACQ effect, methods such as introducing a sterically hindered substituent and employing a twisted and branched molecular structure have been used in the construction of boron-difluoride compounds or other organic luminophores.<sup>[20-24]</sup> The incorporation of various  $\pi$ -conjugated substituents at the *meso*-position of BODIPY perturbs the photophysical and electrochemical properties to a great extent. This perturbation leads to strong absorption with a high molar extinction coefficient, and excellent luminescence properties. Moreover, bulky substituents are introduced in the BODIPY core to keep the individual molecules apart from each other at a certain distance so that close packing of molecules is avoided in the solid state.

In this work, a series of BODIPY compounds was designed with different electron-donating/withdrawing substituents in the *meso*-position. All of the compounds **1a-1e** have rotatable junctions (e.g. 3,5-bis[3',5'-dimethyl phenyl]-phenyl), three benzene rings as rotatable junctions, and these compounds demonstrated a high-emission efficiency in solution. It was found that this series of BODIPY compounds can achieve tunable solid-state fluorescence emission and could be used to make LED device applications, and finally obtain blue-driven LEDs, which makes them promising candidates for the development of efficient light-emitting materials in LED devices.

## 2 | EXPERIMENTAL

### 2.1 | Synthesis

All solvents and reagents were obtained from TCI, Macklin, and the Sinopharm Chemical Reagent Co. Ltd. Tetrahydrofuran (THF) and dichloromethane ( $\text{CH}_2\text{Cl}_2$ ) were distilled over sodium benzophenoneketyl. Silica gel (300-400 mesh) was obtained from the J&K Scientific Ltd.

### 2.2 | General procedure for the synthesis of the BODIPY compound

#### 2.2.1 | Preparation of 3,5-dibromobenzaldehyde (1)

Here, 4 g of 1,3,5-tribromobenzene was added into a round-bottomed flask containing anhydrous THF and placed into a cryogenic coolant circulation pump cooled to  $-78^\circ\text{C}$ . After the temperature was stable,

2.8 ml (2.5 mmol) *n*-butyllithium was added dropwise. The reactant was stirred for 30 min, then 1.2 g *N,N*-dimethylformamide was dropped into the round-bottomed flask and agitated at  $-78^\circ\text{C}$  for 60 min. The container was placed into an ice bath and agitated for 30 min; 15 ml saturated  $\text{NH}_4\text{Cl}$  solution was added to quench the reaction. Then, 50 ml  $\text{CH}_2\text{Cl}_2$  was added, organic solution extraction was completed by brine washing several times, and then a specified amount of anhydrous magnesium sulfate was used to absorb excess water in the solution. A rotary evaporator spiral was used to evaporate the solvent to obtain a coarse product. The crude product was purified by column chromatography with PE:EA = 10:1 as the developing agent. Finally, product **3**, a 5-dibromobenzaldehyde white solid powder was obtained with a yield of 45% (1.98 g).  $^1\text{H-NMR}$  (400 MHz,  $\text{CDCl}_3$ )  $\delta$  9.91 (s, 1H), 7.91 (d,  $J = 12$ , 3H).  $^{13}\text{C-NMR}$  (101 MHz,  $\text{CDCl}_3$ )  $\delta$  189.16, 139.54, 138.86, 131.18, 123.80.

#### 2.2.2 | Preparation of 3,5-dimethylphenylboric (2)

A volume of 50 ml of redistilled tetrahydrofuran was added to a round-bottomed flask, and 5 g of 3,5-dimethylbromobenzene and 3 g of trimethyl borate were added to the flask and placed into a cryogenic coolant circulation pump cooled to  $-78^\circ\text{C}$ . Then, 3 ml (2.5 mmol) *n*-butyllithium were added dropwise and the reactant was stirred for 60 min. Then, the reaction temperature was slowly raised to room temperature and the reaction was continued overnight. The quenching reaction was implemented with 15 ml saturated ammonium chloride solution at an ambient temperature for about 3 h. The organic phase was separated using a separating funnel. The organic solution extraction was completed via brine washing several times, and then a large amount of anhydrous sodium sulfate was used to absorb the excess water in the solution. A rotary evaporator spiral was used to evaporate the solvent to obtain the coarse product, and the coarse product was obtained by column chromatography with a PE:EA = 5:1 solution as the expansion agent and for purification. Finally, the 3,5-dimethylphenylboric white solid powder product was obtained with a yield of 43% (2.2 g).  $^1\text{H-NMR}$  (400 MHz,  $\text{CDCl}_3$ )  $\delta$  7.88 (s, 2H), 7.27 (s, 1H), 2.48 (s, 6H).  $^{13}\text{C-NMR}$  (101 MHz,  $\text{CDCl}_3$ )  $\delta$  137.28, 134.39, 133.30, 131.17, 21.27.

#### 2.2.3 | Preparation of 3,5-bis(3',5'-dimethylphenyl)-benzaldehyde (3)

1,4-Dioxane, water, and potassium carbonate solutions were added to a double-necked circular-bottomed flask containing 2 g 3,5-dimethylphenylboric acid and then 1.76 g 3,5-dibromobenzaldehyde and 608 mg tetraphenylphosphine palladium were added. The reactants were magnetically stirred for a reflux reaction at  $90^\circ\text{C}$  for 12 h in a nitrogen atmosphere. The organic phase was separated using a separating funnel and the water phase was extracted several times using  $\text{CH}_2\text{Cl}_2$ , and then a large amount of anhydrous sodium sulfate was used to absorb the excess water in the

extracted organic solution. A rotary evaporator was used to concentrate the solvent. The crude product was used for column chromatography PE:CH<sub>2</sub>Cl<sub>2</sub> = 15:1, PE:CH<sub>2</sub>Cl<sub>2</sub> = 13:1, PE:CH<sub>2</sub>Cl<sub>2</sub> = 10:1; 500 ml was purified as the eluent, and 3,5-bis(3',5'-dimethylphenyl)-benzaldehyde with a yield of 89.4% (1.87 g) was obtained. <sup>1</sup>H-NMR (400 MHz, CDCl<sub>3</sub>) δ 10.17 (s, 1H), 8.07 (s, 3H), 7.33 (s, 4H), 7.10 (s, 2H), 2.42 (s, 12H). <sup>13</sup>C-NMR (101 MHz, CDCl<sub>3</sub>) δ 192.49, 142.88, 139.79, 138.61, 137.29, 131.85, 129.71, 127.05, 125.15, 21.43.

## 2.2.4 | Compound 1a

In total, 1.29 g 2,4-dimethylpyrrole and 1.7 g 3,5-bis(3',5'-dimethylphenyl)-benzaldehyde were dissolved in anhydrous CH<sub>2</sub>Cl<sub>2</sub> (100 ml) in a N<sub>2</sub> atmosphere. Eight drops of trifluoroacetic acid (TFA) were added to the reaction, and the mixture was stirred overnight. After the reaction was completed through TLC, 1.35 g 2,3-dichloro-5,6-dicyano-1,4-benzoquinone (DDQ) were mixed with redistilled dichloromethane and added to the reaction, which continued for 12 h. Triethylamine (10 ml) was added to the reaction mixture and stirred for 15 min, BF<sub>3</sub>·Et<sub>2</sub>O (10 ml) was added. The reaction mixture was stirred for another 5 h, the mixture was washed several times with water and then extracted with CH<sub>2</sub>Cl<sub>2</sub>. The organic phase was dried over anhydrous sodium sulfate, the coarse product was purified by column chromatography using PE:CH<sub>2</sub>Cl<sub>2</sub> = 6:1, and 2.5 L was purified as an eluent. A difluoro-boron compound of 3,5-bis(3',5'-dimethylphenyl)-phenyl (1a) was obtained as a red powder with a yield of 58% (986 mg). <sup>1</sup>H-NMR (400 MHz, CDCl<sub>3</sub>): δ 7.91 (s, 1H), 7.51 (s, 2H), 7.04 (s, 2H), 6.01 (s, 2H), 2.57 (s, 6H), 2.39 (s, 12H), 1.52 (s, 6H). <sup>13</sup>C-NMR (101 MHz, CDCl<sub>3</sub>) δ 155.58, 143.15, 142.81, 141.66, 140.09, 138.61, 135.74, 131.45, 129.58, 126.20, 124.95, 121.26, 21.42, 14.79. <sup>19</sup>F-NMR (376 MHz, CDCl<sub>3</sub>) δ -146.22 (q, J<sub>B, F</sub> = 67.68 Hz). HRMS (ESI): *m/z* calcd for C<sub>35</sub>H<sub>35</sub>BF<sub>2</sub>N<sub>2</sub><sup>+</sup> [M + H]<sup>+</sup> 533.2961, found 533.2997 (Figure S1).

## 2.2.5 | Compound 1b

A red solid was obtained, yielding 69% <sup>1</sup>H-NMR (400 MHz, CDCl<sub>3</sub>) δ 7.90 (s, 1H), 7.52 (d, J = 4.0, 2H), 6.77 (d, J = 4.0, 4H), 6.51 (t, J = 4.0, 2H), 6.01 (s, 1H), 3.86 (s, 12H), 2.58 (s, 6H), 1.51 (s, 6H). <sup>13</sup>C-NMR (101 MHz, CDCl<sub>3</sub>) δ 161.31, 155.87, 143.07, 142.52, 142.00, 141.29, 135.77, 131.16, 126.37, 125.93, 121.70, 105.35, 99.59, 55.55, 14.86. <sup>19</sup>F-NMR (376 MHz, CDCl<sub>3</sub>) δ -146.23 (q, J<sub>B, F</sub> = 60.16 Hz). HRMS (ESI) *m/z* calcd for C<sub>35</sub>H<sub>35</sub>BFN<sub>2</sub>O<sub>4</sub><sup>+</sup> [M + H]<sup>+</sup> 577.2674, found 577.2624 (Figure S2).

## 2.2.6 | Compound 1c

An orange solid was obtained, yielding 65%. <sup>1</sup>H-NMR (400 MHz, CDCl<sub>3</sub>) δ 7.97 (s, 1H), 7.53 (d, J = 4.0, 2H), 7.51 (s, 6H), 6.02 (s, 2H),

2.59 (s, 6H), 1.55 (s, 6H), 1.39 (s, 36H). <sup>13</sup>C-NMR (101 MHz, CDCl<sub>3</sub>) δ 164.60, 162.16, 156.32, 142.86, 140.96, 139.97, 136.75, 131.00, 126.06, 121.63, 110.21, 109.95, 103.84, 103.19, 14.67. <sup>19</sup>F-NMR (376 MHz, CDCl<sub>3</sub>) δ -146.17 (q, J<sub>B, F</sub> = 67.68 Hz). HRMS (ESI) *m/z* calcd for C<sub>47</sub>H<sub>59</sub>BFN<sub>2</sub><sup>+</sup> [M + H]<sup>+</sup> 681.4749, found 681.4751 (Figure S3).

## 2.2.7 | Compound 1d

A red solid was obtained, yielding 63%. <sup>1</sup>H-NMR (400 MHz, CDCl<sub>3</sub>) δ 7.84 (s, 1H), 7.56 (d, J = 4.0, 2H), 7.15 (dd, J = 8.0, 4H), 6.84–6.89 (m, J = 4.0, 2H), 6.03 (s, 2H), 2.58 (s, 6H), 1.48 (s, 6H). <sup>13</sup>C-NMR (101 MHz, CDCl<sub>3</sub>) δ 155.57, 151.64, 143.56, 143.29, 141.77, 139.47, 135.75, 131.51, 126.86, 125.22, 122.29, 121.41, 121.33, 35.07, 31.53, 14.79. <sup>19</sup>F-NMR (376 MHz, CDCl<sub>3</sub>) δ -146.22 (q, J<sub>B, F</sub> = 67.68 Hz), -108.61 (s). HRMS (ESI) *m/z* calcd for C<sub>31</sub>H<sub>23</sub>BF<sub>5</sub>N<sub>2</sub><sup>+</sup> [M + H]<sup>+</sup> 529.1869, found 529.1865 (Figure S4).

## 2.2.8 | Compound 1e

A red solid was obtained, yielding 62%. <sup>1</sup>H-NMR (400 MHz, CDCl<sub>3</sub>) δ 8.06 (s, 4H), 7.96 (s, 2H), 7.93 (s, 1H), 7.70 (s, 2H), 6.06 (s, 2H), 2.59 (s, 6H), 1.51 (s, 6H). <sup>13</sup>C-NMR (101 MHz, CDCl<sub>3</sub>) δ 156.59, 142.47, 141.48, 140.63, 139.08, 137.66, 133.25, 132.92, 132.59, 132.19, 131.18, 127.48, 127.25, 126.46, 124.49, 122.15, 121.82, 46.67, 15.03, 14.67, 8.72. <sup>19</sup>F-NMR (376 MHz, CDCl<sub>3</sub>) δ -146.20 (q, J<sub>B, F</sub> = 63.92 Hz), -62.66 (s). HRMS (ESI) *m/z* calcd for C<sub>35</sub>H<sub>24</sub>BF<sub>14</sub>N<sub>2</sub><sup>+</sup> [M + H]<sup>+</sup> 749.1803, found 749.1808 (Figure S5).

## 2.3 | DFT calculations

Molecular calculations were implemented in the Gaussian 09 program.<sup>[28,29]</sup> The ground states of the compounds 1a–1e were fully optimized by a functional (B3LYP) and basis set 6-31G\*.

## 2.4 | Fabrication of blue-driven LEDs

The chip emits a blue light at around 470 nm. The filling ratio (C:compound) of the compound in the glue is A:B:C = 100:10:40 (mg). The mixture was stirred in the same direction, and air bubbles were removed by vacuum for 15 min, and the mixture then deposited on the LED chip. Electroluminescence spectra of the LEDs were implemented at 125.9°C using an Everfine HAAS-2000 instrument, the LED with a forward current range from 300 to 350 mA. To gather light, the LED was placed in an integrating sphere with a diameter of 30 cm, and coupled to a high-precision array with a spectroradiometer (wavelength accuracy < 0.3 nm) and a programmable test power supply LED 300.

### 3 | RESULTS AND DISCUSSION

#### 3.1 | Synthesis and characterization

The synthetic routes of compounds **1a–1e** are illustrated in Scheme 1. To adjust the photophysical properties of the compounds, varied electron-donating/withdrawing substituents were connected to the BODIPY  $\pi$ -conjugation cores via phenyl units, which produced good yields (over 60%). All target compounds were soluble in  $\text{CH}_2\text{Cl}_2$ , tetrahydrofuran (THF), toluene, *N,N*-dimethylformamide (DMF) and air stable.  $^1\text{H-NMR}$ ,  $^{13}\text{C-NMR}$ ,  $^{19}\text{F-NMR}$ , and mass spectroscopy confirmed the proposed structures for compounds **1a–1e**.

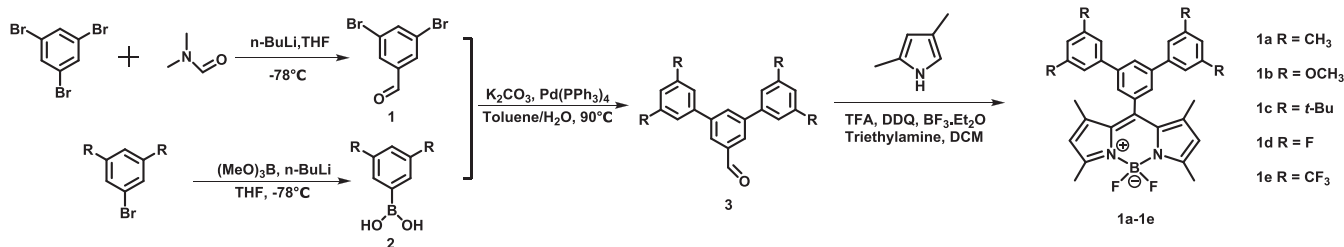
#### 3.2 | Electronic absorption in solution and solid state

The UV-vis absorption of compounds **1a–1e** obeys the Lambert-Beers law in the concentration range of this study ( $1 \times 10^{-6}$  to  $1 \times 10^{-4}$  mol  $\text{L}^{-1}$ ) in  $\text{CH}_2\text{Cl}_2$  (Figure S8), illustrating that no aggregation occurred at this concentration range. The optical data measured in different solvents are listed in Table 1 and the UV-vis absorption spectra of **1a–1e** in  $\text{CH}_2\text{Cl}_2$  are presented in Figure 1. All these compounds showed strong and sharp absorption bands between 420 to 530 nm, which were attributed to the  $^1\pi-\pi^*$  transitions localized on the BODIPY aromatic rings.<sup>[25]</sup> Compounds **1d** and **1e** connect withdrawing substituents that show a slight bathochromic shift and can be ignored. In addition, the photophysical properties of these BODIPYs

were measured in five solvents with different polarities: acetonitrile (ACN), tetrahydrofuran (THF), dichloromethane (DCM), toluene (TL), and hexane (HEX) (Figure S6). A similar phenomenon was observed for compounds **1a–1e**, and all of the compounds exhibited minor solvatochromic effects, as shown in Figure S6. This minor solvatochromic effect also supported the  $^1\pi-\pi^*$  distribution of their absorption bands. In addition, compared with their absorption spectra in solution, the electron-donating/withdrawing substituents connected to BODIPY had a minor influence on their electronic absorption. The absorption properties of compounds **1a–1e** were also measured in the solid state (Figure 1b), which showed strong absorption bands ranging from 430 to 550 nm. Compared with the UV-vis absorption measured in solution, the maximum absorption wavelengths (504–525 nm) were red-shifted, and the absorption bands were broader than those obtained in solution. Compared with **1a**, the solid-state absorptions of compound **1c** with *t*-Bu groups and **1e** with trifluoromethyl groups exhibited obvious blue shifts. This could be attributed to the greater steric hindrance of these substituents than methyl groups. Therefore, the  $\pi-\pi$  stacking effect among the molecules could be reduced, which produced the blue shift of their solid-state absorptions.

#### 3.3 | Photoluminescence in solution and solid state

The photoluminescence properties of compounds **1a–1e** in different solvents were tested (Figure S7), and their normalized emission spectra in  $\text{CH}_2\text{Cl}_2$  ( $1 \times 10^{-5}$  mol  $\text{L}^{-1}$ ) are shown in Figure 2. The emission



**SCHEME 1** The general synthetic route of the BODIPYs

**TABLE 1** Optical data measured in different solvents at room temperature

Solvent	1a			1b			1c			1d			1e		
	$\lambda_{\text{ab}}$ (nm)	$\lambda_{\text{em}}$ (nm)	$\Phi_{\text{F}}^{\text{a}}$	$\lambda_{\text{ab}}$ (nm)	$\lambda_{\text{em}}$ (nm)	$\Phi_{\text{F}}^{\text{a}}$	$\lambda_{\text{ab}}$ (nm)	$\lambda_{\text{em}}$ (nm)	$\Phi_{\text{F}}^{\text{a}}$	$\lambda_{\text{ab}}$ (nm)	$\lambda_{\text{em}}$ (nm)	$\Phi_{\text{F}}^{\text{a}}$	$\lambda_{\text{ab}}$ (nm)	$\lambda_{\text{em}}$ (nm)	$\Phi_{\text{F}}^{\text{a}}$
Hexane	501	514	0.94	501	515	0.97	501	514	0.96	503	517	0.89	504	518	0.97
Toluene	504	519	0.95	505	520	0.95	502	519	0.91	506	521	0.98	508	523	0.99
DCM	502	516	0.96	502	517	0.94	501	516	0.98	503	518	0.95	504	519	0.98
THF	501	515	0.98	501	515	0.95	501	514	0.98	502	516	0.97	503	517	0.96
Acetonitrile	498	512	0.92	498	512	0.92	498	512	0.96	499	513	0.88	499	513	0.93

<sup>a</sup> $\Phi_{\text{F}}$  (absolute fluorescence quantum yield) was determined in different solvents. Abbreviations:  $\lambda_{\text{ab}}$  = absorption maximum,  $\lambda_{\text{em}}$  = emission maximum, were determined in different solvents ( $1 \times 10^{-5}$  M) at room temperature.

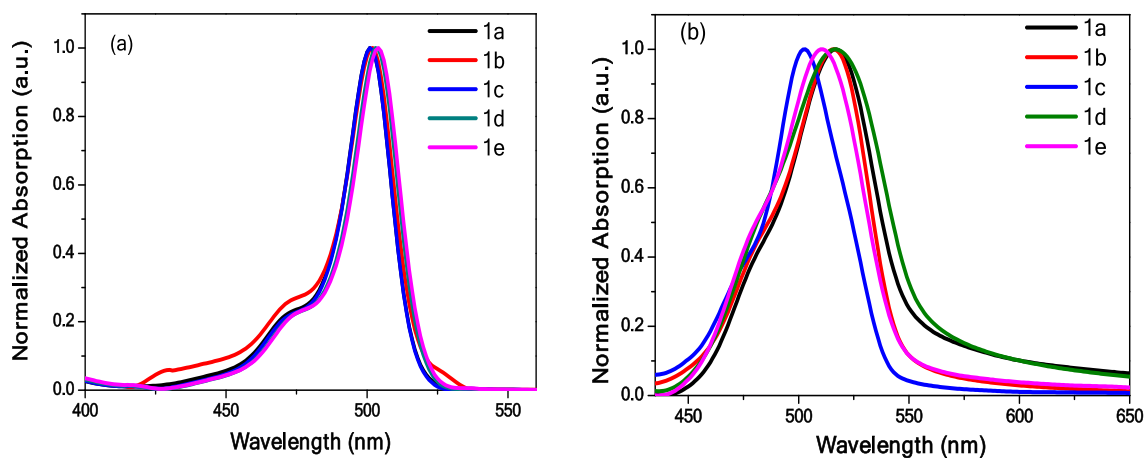


**FIGURE 1** (a) Normalized UV-vis absorption spectra of **1a–1e** in  $\text{CH}_2\text{Cl}_2$  ( $1 \times 10^{-5}$  M) at room temperature. (b) Normalized UV-vis absorption spectra of **1a–1e** in the solid state

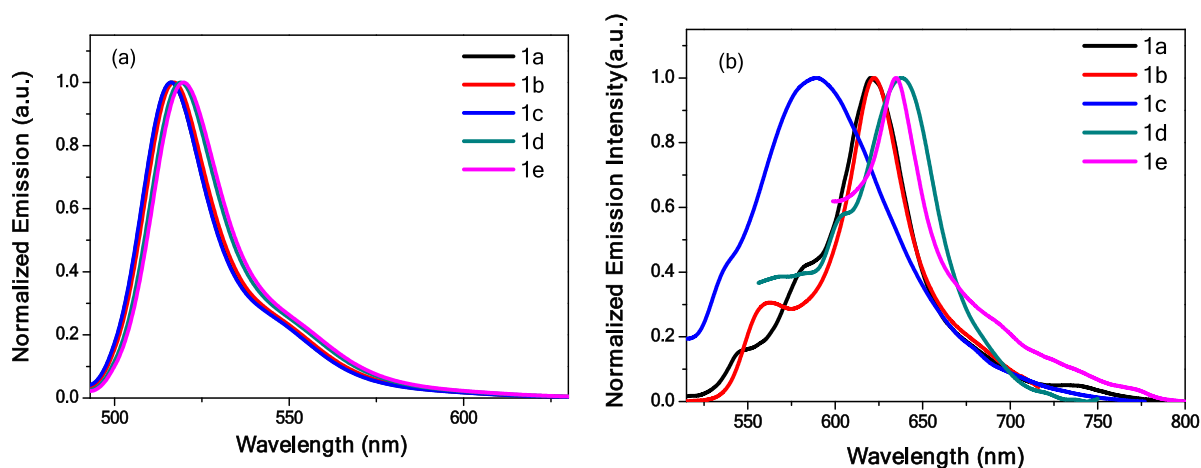


**FIGURE 2** (a) Normalized emission spectra of **1a–1e** in  $\text{CH}_2\text{Cl}_2$  ( $1 \times 10^{-5}$  M). (b) Normalized emission spectra of **1a–1e** in the solid state

**TABLE 2** Experimental data of photophysical properties of compounds **1a–1e** in the solid state

Compound	$\lambda_{\text{ab}}$ nm	$\lambda_{\text{em}}$ nm	$\Phi_f$ %	$\tau_{\text{av}}$ ns	$k_r^{\text{a}}$ ns $^{-1}$	$k_{\text{nr}}^{\text{b}}$ ns $^{-1}$
<b>1a</b>	518	620	18.4	2.8	0.066	0.291
<b>1b</b>	517	619	5.3	2.6	0.020	0.364
<b>1c</b>	504	575	1.5	2.4	0.006	0.410
<b>1d</b>	520	640	0.1	2.2	0.0005	0.454
<b>1e</b>	512	645	1.2	2.3	0.005	0.429

<sup>a</sup>Radiative rate constant  $k_r = \Phi_f / \tau_{\text{av}}$ .

<sup>b</sup>Nonradiative rate constant  $k_{\text{nr}} = (1 - \Phi_f) / \tau_{\text{av}}$ .

band maxima and photoluminescence quantum yields are listed in Table 1. All compounds shared different photoluminescence quantum yields in solution ( $\Phi_{\text{PL}} = 88\text{--}99\%$ ) and the solid state ( $\Phi_f = 0.1\text{--}18.4\%$ ) (Table 2). As shown in Figure 2a, compounds **1a–1e** emitted a green light in a  $\text{CH}_2\text{Cl}_2$  solution and exhibited quite small Stokes' shifts ( $\sim 15$  nm). Considering these characteristics, we could attribute the emission to the  $^1\pi\text{--}\pi^*$  transition. The compounds **1d** and

**1e** exhibited slight bathochromic shifts ( $< 5$  nm), which connected electron-withdrawing substituents (F and  $\text{CF}_3$ ). Moreover, the bathochromic shifts of emissions could be explained by the decreased energy band gap (Table 3). The compounds **1a–1c** connecting electron-donating substituents (such as  $\text{CH}_3$ ,  $\text{OCH}_3$ , and *t*-Bu) showed a similar emission performance, and this was almost identical to the UV-vis absorption spectra that we obtained.

As shown in Figure 2b, the emission bands of the solid fluorescence of compounds **1a–1e** were broader than those in solution. Compared with **1a** and **1b**, compounds **1d** and **1e** bearing electron-withdrawing groups showed minor bathochromic shifts (13 and 16 nm). This phenomenon was similar to the photoluminescence in  $\text{CH}_2\text{Cl}_2$ . However, the emission of compound **1c** was quite blue-shifted compared with that of other compounds, which is also consistent with the observation of their solid-state absorption. In addition, **1c** showed a broader emission band; the steric hinderance of the molecule increased due to the bulky *tert*-butyl groups and decreased the intermolecular  $\pi$ - $\pi$  stacking interaction. This made it difficult to delocalize  $\pi$ -electrons, therefore **1c** required more energy for emission in the accumulation and showed a hypsochromic shift. Compared with the emission spectra in solution, broader emission bands with considerable bathochromic shifts (except **1c**) were observed in the solid state, which indicated that the  $\pi$ - $\pi$  stacking of the planar configurations of the BODIPY compound in solid state led to an increase in the  $\pi$ -conjugation length. The solid-

state fluorescence quantum yields of these complexes were less than 20%. This could be attributed to the strong  $\pi$ - $\pi$  interaction between the molecules, which produced excimer complexes that were not conducive to luminescence, resulting in a decrease in fluorescence quantum yield.<sup>[26]</sup> The complexes with electron-donating groups were slightly beneficial for the enhancement of solid-state fluorescence.

### 3.4 | Theoretical calculations and electrochemistry

The ground-state electron density distribution of the highest occupied molecular orbital (HOMO) and lowest unoccupied molecular orbital (LUMO) are illustrated in Figure 3. The HOMO-LUMO energy differences (energy band gaps, calculated  $E_g^{\text{cal}}$ ) are presented in Table 2. Compounds **1a–1c** possessed almost the same values for the HOMO ( $-2.35$ – $-2.36$  eV) and LUMO ( $-5.40$ – $-5.41$  eV), while the band gap of compounds **1d** and **1e** were the largest with a HOMO of ( $-2.60$ – $-2.75$  eV) and a LUMO of ( $-5.63$ – $-5.76$  eV). Due to the coplanar configuration, the  $\pi$ -electrons in the HOMO of compounds **1a–1e** were distributed on the BODIPY cores, Strong orbital interactions could be generated among the stacked  $\pi$ -systems. While their LUMOs showed almost no change compared with the HOMOs, the  $\pi$ -electrons in the LUMO of compounds **1d** and **1e** had a tendency to shift to *meso*-position substituents. Furthermore, observation of the ground-state optimized structures through the compounds **1a–1e**, the dihedral angles between the aromatic rings, and the cores were studied. For instance, the dihedral angle between the aromatic ring of **1a** and its BODIPY core unit was  $90^\circ$ , as illustrated in Figure 4. This

TABLE 3 DFT calculation results of HOMO-LUMO energy levels

Compound	LUMO (eV)	HOMO (eV)	$E_g^{\text{cal}}$ (eV) <sup>a</sup>
<b>1a</b>	-2.36	-5.41	3.05
<b>1b</b>	-2.35	-5.40	3.05
<b>1c</b>	-2.35	-5.40	3.05
<b>1d</b>	-2.60	-5.63	3.03
<b>1e</b>	-2.75	-5.76	3.01

<sup>a</sup>Carried out at the B3LYP/6-31G\* level of theory.

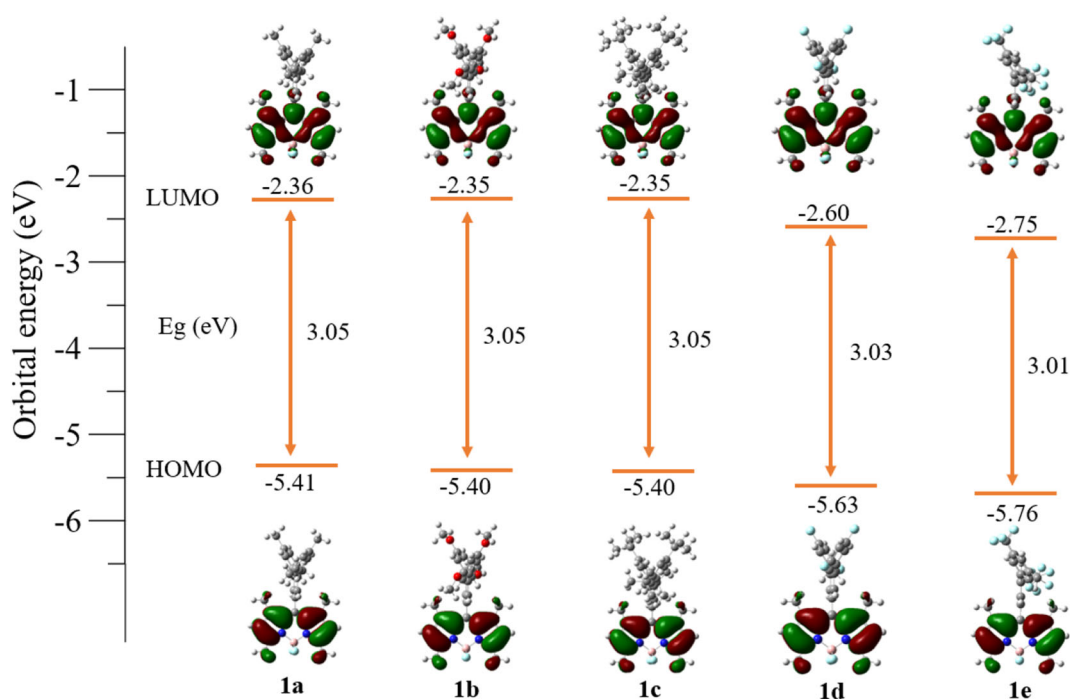
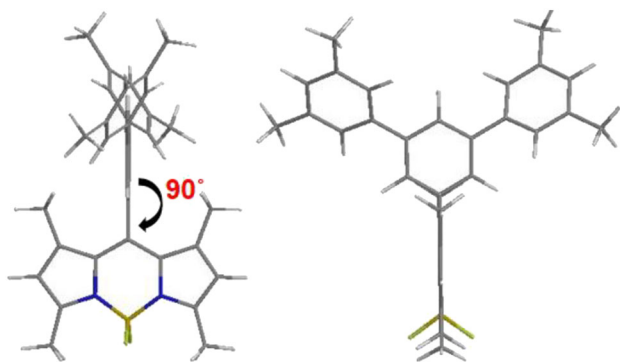


FIGURE 3 Molecular orbital surfaces of the HOMOs and LUMOs for **1a–1e** obtained at the B3LYP/6-31G\* level



large dihedral angle made it difficult for electrons in molecules to form an effective delocalization. The above results indicated that the intermediate bridging group, either the strong electron donor or the strong electron acceptor, could not produce a significant intramolecular charge transfer for the whole molecule. Therefore, there was no significant bathochromic shift in the absorption spectrum. Aryl substituents introduced onto the *meso*-carbon generally produce a slight effect on the HOMO and LUMO energy levels.<sup>[27]</sup> In addition, the electrochemical properties of compounds **1a–1e** were investigated using cyclic voltammetry. The electrochemical potentials and energy levels of these compounds are shown in Table 4, and although the theoretically calculated  $E_g^{\text{cal}}$  value (3.01–3.05 eV) was significantly higher than the energy gap  $E_g^{\text{opt}}$  (2.32–2.34 eV) obtained from the ground-state absorption, the changing trend of the compound energy gap remained consistent.



**FIGURE 4** Dihedral angle of the ring between the aromatic ring and the core according to the ground-state optimized structure of **1a**

**TABLE 4** Electrochemical potentials and energy levels of compounds **1a–1e**

Compound	$E_{\text{ox}}$ (V) <sup>a</sup>	$E_{\text{red}}$ (V) <sup>a</sup>	HOMO (eV) <sup>b</sup>	LUMO (eV) <sup>c</sup>	$E_g$ (eV) <sup>d</sup>
<b>1a</b>	0.54	−0.51	5.34	3.00	2.34
<b>1b</b>	0.59	−0.56	5.39	3.06	2.33
<b>1c</b>	1.18	−0.22	5.98	3.64	2.34
<b>1d</b>	0.58	−0.40	5.38	3.06	2.32
<b>1e</b>	0.95	—	5.75	3.43	2.32

<sup>a</sup>Potentials determined by cyclic voltammetry in a deoxygenated solution of THF, containing 0.1 M TBAP, at a concentration of  $10^{-3}$  M, at room temperature. Potentials were standardized with a ferrocene-ferrocenium (Fc/Fc<sup>+</sup>) couple as the internal reference vs Ag/AgNO<sub>3</sub>. Scan rate 0.1 V/s. Working electrode: glassy carbon, counter electrode: Pt wire, reference electrode: Ag/AgNO<sub>3</sub>. <sup>b</sup>HOMO =  $E_{\text{ox}} + 4.8$  eV. <sup>c</sup>LUMO = HOMO −  $E_g$ . <sup>d</sup> $E_g$  estimated from the UV–vis absorption spectra.

### 3.5 | LED devices

Compounds **1a–1e** were applied to LEDs actuated by a blue LED chip. The electroluminescence measurement results are listed in Table 5. The colour rendering index (CRI) values of these LEDs ranged from 33 to 66, which confirmed that different emissions could be achieved via the fabrication of LEDs based on compounds **1a–1e** (Figure 5). Among these, the CRI value of the LED device constructed by compound **1e** exceeded 60, therefore exhibiting a blue emission property. Compound **1d** showed the highest luminescence efficiency (up to 34 lm/W) compared with other compounds. The dominant wavelength of each device on the electroluminescence spectrum was in the range of 469–605 nm, which could change the colour of the device from blue to orange by blue-driven LEDs. In addition, the correlated colour temperature (CCT) of these LEDs could be revised from 1130 K to 83 060 K, which realized the control of cold and warm colour temperatures. The CIE coordinate plot are shown in Figure S9, and accurate values are listed in Table 5. Five devices were made from this series of compounds, their CIE coordinate values not only indicated the luminescence colour, but also were related to the luminescence efficiency. When the X value of the CIE coordinate was less than 0.3, the luminescence efficiency of the other four devices (except device **1b**) was greater than 10%. Furthermore, the Y value of the four devices was greater than 0.3, and the luminescence efficiency was further increased. By comparison, it was found that the X value of the CIE coordinates was less than 0.3 and the Y value was greater than 0.3, therefore the device emitted high luminescence efficiently under a low loading amount. These results also provide a basis for designing BODIPY complexes rationally with intensive emission for light-emitting applications.

**TABLE 5** Electroluminescence data of LEDs based on compounds **1a–1e**

Device	<b>1a</b>	<b>1b</b>	<b>1c</b>	<b>1d</b>	<b>1e</b>
CIE	(0.29, 0.37)	(0.42, 0.36)	(0.23, 0.38)	(0.19, 0.36)	(0.20, 0.26)
CCT (K)	2150	1136	3163	4434	83 060
CRI	33	48	33	43	66
Luminescence efficiency (lm/W)	16.46	1.09	21.19	34.13	10.19
Photoelectric efficiency (%)	4.273	0.635	4.463	7.730	4.180

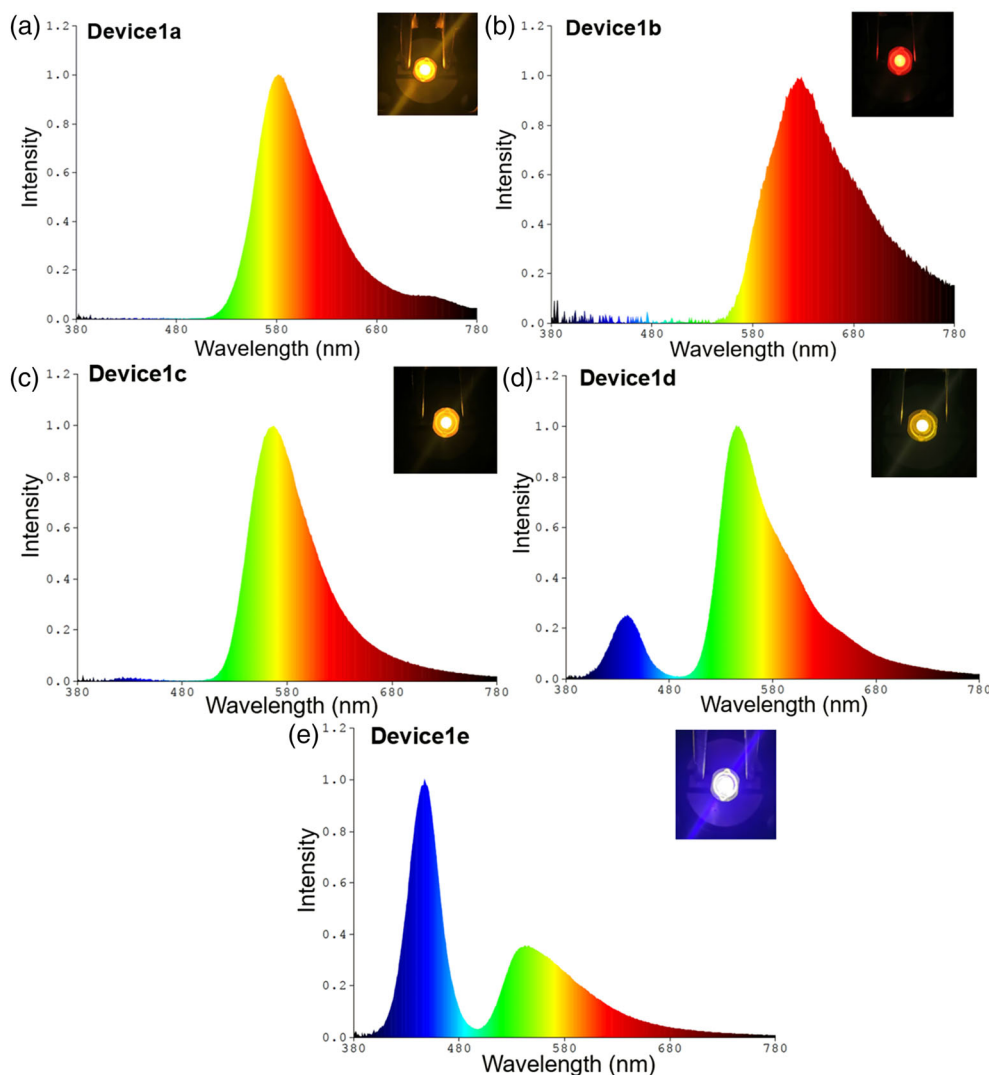


**FIGURE**  
5 Electroluminescence spectra of LED devices 1a–1e (a–e). Inset: Photographs of devices 1a–1e with forward current

## 4 | CONCLUSION

A series of BODIPY compounds (1a–1e) with different electron-donating/withdrawing aromatic substituents was designed and synthesized. Their absorption and emission spectra were recorded in different solvents and in the solid state. Compounds 1a–1e exhibited strong  ${}^1\pi\text{-}\pi^*$  absorption in the visible spectral region and exhibited intense green  ${}^1\pi\text{-}\pi^*$  emissions with relatively high photoluminescence quantum yields (>0.9). Moreover, these compounds showed a minor difference for their  $E_g^{\text{cal}}$  value (3.01–3.05 eV), which was caused by the large dihedral angles between the aromatic substituents and the cores. However, when these compounds were applied to blue-driven LEDs as light-emitting materials, they exhibited different solid-state fluorescence properties and produced blue to orange emissions. These results provide a good guide that is significant not only for the synthesis of efficient fluorescent materials by introducing twisted groups at the meso-position of BODIPY, but also for the design and potential construction of colour-tunable LEDs.

## ACKNOWLEDGEMENTS

The authors greatly acknowledge the Natural Science Foundation of Jiangsu Province (BK20170104), the National Natural Science Foundation of China (21602106), ‘Six Talent Peaks Project’ of Jiangsu Province (XCL-037) and Postgraduate Research & Practice Innovation Programme of Jiangsu Province (KYCX20\_1032) for financial support.

## ORCID

Rui Liu  <https://orcid.org/0000-0002-8227-6064>

## REFERENCES

- [1] A. Treibs, F. H. Kreuzer, *Liebigs Ann Chem.* **1968**, 718, 208.
- [2] A. Loudet, K. Burgess, *Chem. Rev.* **2007**, 107, 4891. <https://doi.org/10.1021/cr078381n>
- [3] T. M. Sudesh, K. Jin, L. Yunho, G. C. David, *Org. Lett.* **2014**, 16, 520. <https://doi.org/10.1021/ol403405n>
- [4] W. Ryan, P. Candace, A. Jeffrey, *J. Org. Chem.* **2010**, 75, 2883. <https://doi.org/10.1021/jo100095n>
- [5] B. D. Ana, H. J. Xu, Z. L. Xue, H. Katrin, Z. Shen, G. W. Michael, X.-Z. You, K. Rurack, *Org. Lett.* **2008**, 10, 1581. <https://doi.org/10.1021/ol800271e>



- [6] K. Syam K, B. Christoffer, J. A. D. Good, M. Shamil, C. Erik, B. A. Lennart, F. Almqvist, *J. Org. Chem.* **2013**, *78*, 12207. <https://doi.org/10.1021/jo401844y>
- [7] W. J. Shi, P. C. Lo, S. Anu, L. R. Isabelle, *Tetrahedron* **2012**, *68*, 8712. <https://doi.org/10.1016/j.tet.2012.08.033>
- [8] L. M. Michael, J. Lu, A. G. Richard, *Science* **1996**, *271*, 1420. <https://doi.org/10.1126/science.271.5254.1420>
- [9] A. F. Steven, P. Michael, S. Y. Ho, D. J. Lain, S. W. Daniel, *Science* **2001**, *292*, 1385. <https://doi.org/10.1126/science.1060418>
- [10] U. Gilles, Z. Raymond, H. Anthony, *Angew. Chem., Int. Ed.* **2008**, *47*, 1184.
- [11] Z. Raymond, U. Gilles, H. Anthony, *New J. Chem.* **2007**, *31*, 496. <https://doi.org/10.1039/B617972J>
- [12] S. Makoto, N. Takashi, U. Junji, Y. Masaki, *Chem. Commun.* **2016**, *52*, 10727. <https://doi.org/10.1039/C6CC05439K>
- [13] L. G. Boris, M. Olivier, J. Denis, *Phys. Chem. Chem. Phys.* **2012**, *14*, 157. <https://doi.org/10.1039/C1CP22396H>
- [14] R. Hu, L. Erik, A.-A. Ange'lica, J. Liu, J. W. Y. Lam, D. W. Ian, Y. Zhong, K. S. Wong, E. Peña-Cabrera, B. Z. Tang, *J. Phys. Chem. C* **2009**, *113*, 15845. <https://doi.org/10.1021/jp902962h>
- [15] K. Katerina, C. Gonzalo, *J. Am. Chem. Soc.* **2010**, *132*, 17560. <https://doi.org/10.1021/ja1075663>
- [16] P. Antonio, F. Alberto, C. Clemence, *Phys. Chem. Chem. Phys.* **2016**, *18*, 32668. <https://doi.org/10.1039/C6CP06799A>
- [17] B. Jorge, J. A. Ismael, V. E. Ismael, A. H. Alejandro, *RSC Adv.* **2011**, *1*, 677. <https://doi.org/10.1039/C1RA00020A>
- [18] J. A. Ismael, R. Hu, B. Z. Tang, I. L. Fabiola, P. C. Eduarodo, *Tetrahedron* **2011**, *67*, 7244. <https://doi.org/10.1016/j.tet.2011.07.067>
- [19] L. Y. Jiao, C. J. Yu, M. Liu, Y. Wu, K. B. Cong, *J. Org. Chem.* **2010**, *75*, 6035. <https://doi.org/10.1021/jo101164a>
- [20] T. P. I. Saragi, S. Till, S. Achim, F. L. Thomas, S. Josef, *Chem. Rev.* **2007**, *107*, 1011. <https://doi.org/10.1021/cr0501341>
- [21] X. F. Mei, J. W. Wang, Z. G. Zhou, S. Y. Wu, L. M. Huang, Z. H. Lin, Q. Ling, *J. Mater. Chem. C* **2017**, *5*, 2135. <https://doi.org/10.1039/C6TC05519B>
- [22] J. P. Wang, Y. Qi, X. L. Niu, H. Tang, *J. Nutr. Biochem.* **2018**, *54*, 130. <https://doi.org/10.1016/j.jnutbio.2017.12.004>
- [23] Y. Wan, J. Li, X. Peng, *RSC Adv.* **2017**, *7*, 35543. <https://doi.org/10.1039/c7ra06237k>
- [24] J. Li, C. Yang, X. Peng, *J. Mater. Chem. C* **2018**, *6*, 19. <https://doi.org/10.1039/c7tc03780e>
- [25] H. Lu, M. John, Y. C. Yang, Z. Shen, *Chem. Soc. Rev.* **2014**, *43*, 4778. <https://doi.org/10.1039/C4CS00030G>
- [26] W. Christoph, S. W. Mark, *Macromolecules* **1996**, *29*, 5157. <https://doi.org/10.1021/ma950902y>
- [27] M. Josef, *J. Am. Chem. Soc.* **1978**, *100*, 6801. <https://doi.org/10.1021/ja00490a001>
- [28] D. B. Axel, *J. Chem. Phys.* **1992**, *96*, 2155. <https://doi.org/10.1063/1.462066>
- [29] M. F. Michelle, J. P. William, J. H. Warren, *J. Chem. Phys.* **1982**, *77*, 3654. <https://doi.org/10.1063/1.444267>

#### SUPPORTING INFORMATION

Additional supporting information may be found online in the Supporting Information section at the end of this article.

**How to cite this article:** H. Liu, H. Su, Z. Chen, S. Zhu, R. Liu, H. Zhu, *Luminescence* **2021**, *1*, <https://doi.org/10.1002/bio.4111>